Time-Resolved Photoelectron Spectra of CS_2: Dynamics at Conical Intersections

Kwanghsi Wang, and Vincent McKoy*
A. A. Noyes Laboratory of Chemical Physics, California Institute of Technology, Pasadena, California 91125, USA

Paul Hockett, and Michael S. Schuurman†
National Research Council of Canada, 100 Sussex Drive, Ottawa, Ontario K1A 0R6, Canada

(Received 19 May 2013; revised manuscript received 6 January 2014; published 21 March 2014)

We report results of the application of a fully *ab initio* approach for simulating time-resolved molecular-frame photoelectron angular distributions around conical intersections in CS_2. The technique employs wave packet densities obtained with the multiple spawning method in conjunction with geometry- and energy-dependent photoionization matrix elements. The robust agreement of these results with measured molecular-frame photoelectron angular distributions for CS_2 demonstrates that this technique can successfully elucidate, and disentangle, the underlying nuclear and photoionization dynamics around conical intersections in polyatomic molecules.

DOI: 10.1103/PhysRevLett.112.113007 PACS numbers: 33.60.+q, 82.20.Gk, 82.53.Eb, 82.53.Kp

Time-resolved photoelectron spectroscopy (TRPES) is a versatile probe of ultrafast dynamics in molecules and has been used extensively in recent years to study nonadiabatic dynamics processes in numerous systems [1–7]. The sensitivity of the method to changes in both the motion of the nuclei as well as the evolution of the electronic structure of molecules makes it particularly well suited for studies of wave packet dynamics around conical intersections where the nuclear and electronic degrees of freedom are coupled. Conical intersections, and nonadiabatic transitions in general, are central to the efficiency of photobiological processes, such as vision [8] and photosynthesis [9], and are believed to be responsible for the photostability of the DNA bases under ultraviolet radiation [10].

In cases where the electronic-nuclear mixing cannot be unambiguously interrogated on the basis of the photoelectron energy alone, molecular-frame photoelectron angular distributions can be used to track nuclear dynamics and discern the electronic character of the underlying states [11–15]. In this Letter, we report the results obtained employing a general framework for simulating time-resolved photoelectron angular distributions (PADs) that incorporates the first-principles treatment of the nuclear dynamics with the photoionization dynamics, while remaining practical for applications involving molecules large enough to have interesting photochemistry. The simulation of the nuclear dynamics is described using the *ab initio* multiple spawning (AIMS) method [16–18], which is a time-dependent formulation of quantum chemistry that propagates vibronic trajectories on potential energy surfaces determined "on the fly." The wave packet densities from these simulations, at a series of time delays, are subsequently employed in conjunction with the computed photoionization amplitudes [19] between the underlying neutral electronic states and the ionic continua in order to produce an energy-and angle-resolved TRPES spectrum. While previous, fully quantum, dynamical studies have demonstrated the efficacy of our method for computing photoionization amplitudes in time-resolved studies of di- and triatomic molecules [5,20,22,23,25], coupling this formalism to AIMS wave packet simulations allows for the treatment of general polyatomic systems.

Recently, Bisgaard and co-workers [15,21] studied time-resolved molecular-frame PADs (TRMFPADs) to monitor the evolution of the electronic character of the excited state wave packet in a nonadiabatic photodissociation reaction of CS_2. The observed temporal evolution of the TRMFPADs was attributed to mixing of the initially prepared excited state ($^1\Sigma_u^+$) in the Franck-Condon region with a close-lying dark state ($^1\Pi_g$) as the molecule bends and stretches. These seminal studies illustrated the potential of TRMFPADs for characterizing nonadiabatic dynamics in molecular systems.

Figure 1 shows the potential surfaces for a few of the lowest $^1A'$ states of neutral CS_2 along the C–S antisymmetric stretch coordinate for bond angles of 1(a) 180° 1(b) 160°, and 1(c) 140° with the other C–S bond length fixed at 3.0 a.u. Curve crossings between these electronic states are clearly evident, forming seams of conical intersection. Between 3 and 5 a.u. the adiabatic S_2 state is a strong admixture of the $^1\Sigma_u^+$, $^1\Pi_g$, and $^1\Delta_u$ states. A triplet dissociative state crossing around the basin of the $S_2(^1\Sigma_u^+)$ state is not shown. Though triplet dissociation products are observed spectroscopically [15,21], intersystem crossing to the triplet manifold is not expected to figure heavily in the early-time dynamics. The agreement between the measured MFPADs and those calculated here ignoring the triplet states indicates that this assumption is reasonable. However, if it were necessary to include spin-orbit coupling, the AIMS method also allows for wave packet propagation on spin-orbit coupled surfaces.

In the AIMS method, the total wave function is expanded as a sum of products of nuclear basis functions and

adiabatic electronic wave functions. The nuclear basis functions are chosen to be complex multidimensional products of frozen Gaussians [26], parametrized by their average positions and momenta (which evolve according to Hamilton's equation) and a semiclassical phase factor (which evolves as the time integral of the classical Lagrangian). The coefficients in the expansion of the total wave function are determined variationally from the solution of the time-dependent nuclear Schrödinger equation. Propagation of the nuclear basis functions is performed using energy gradients and nonadiabatic couplings determined from *ab initio* electronic structure methods at each time step. Since the vibronic wave packet is defined in Cartesian coordinates, and requires only the local properties of the potential energy surface in order to propagate trajectories, the formalism is very flexible and can be applied to the study of large polyatomic molecules of photochemical interest such as uracil, thymine, and protein chromophores [16,17]. The representation of the potential energy surface is, in fact, formally independent of the AIMS propagation procedure, and the actual choice of the potential can be motivated by computational, chemical, or other considerations.

In this study, the initial positions and momenta of the Gaussian basis functions were sampled from the ground-state Wigner distribution, subject to the constraint that $|E(R_{S_2}) - E(R_{S_0}) - h\nu_{\text{pump}}| \leq \text{FWHM}_{\text{pump}}$ (the estimated bandwidth of the pump pulse) and then vertically lifted onto the $C^1\Sigma_u^+$ (S_2) excited state surface. The simulation thus assumes a short pulse in time (and very broad in energy) but filters the initial conditions such that the excitation energy at $t = 0$ lies within the experimental energy bandwidth.

The potential energy surfaces shown in Fig. 1 were obtained from a multireference configuration interaction (MRCI) [27] calculation and using correlation consistent polarized double zeta basis sets [28]. The MRCI calculation employed 10 complete active space self-consistent field orbitals and 14 electrons. The potential energy surfaces for the lowest $^2A'$ and $^2A''$ ionic states are obtained from similar calculations. The ionic surfaces are shifted up by 0.511 eV to yield the measured value of the vertical ionization potential of the $C^1\Sigma_u^+$ state at the equilibrium geometry of the ground state. These potential surfaces are nearly identical to those used in the AIMS simulation, which employed MRCI computations [29], a 10 electron/8 orbital complete active space self-consistent field reference, and atomic natural orbital basis sets [30].

The simulations show that at early times the wave packet splits into two parts and moves away from the Franck-Condon region along the symmetric and antisymmetric stretching coordinates, with some dissociation beginning as early as 70 fs along the antisymmetric stretching coordinate. Part of the wave packet gradually evolves along the bending coordinate while motion along the faster antisymmetric and symmetric stretching brings the wave packet back to the Franck-Condon region. This process is repeated and results in some

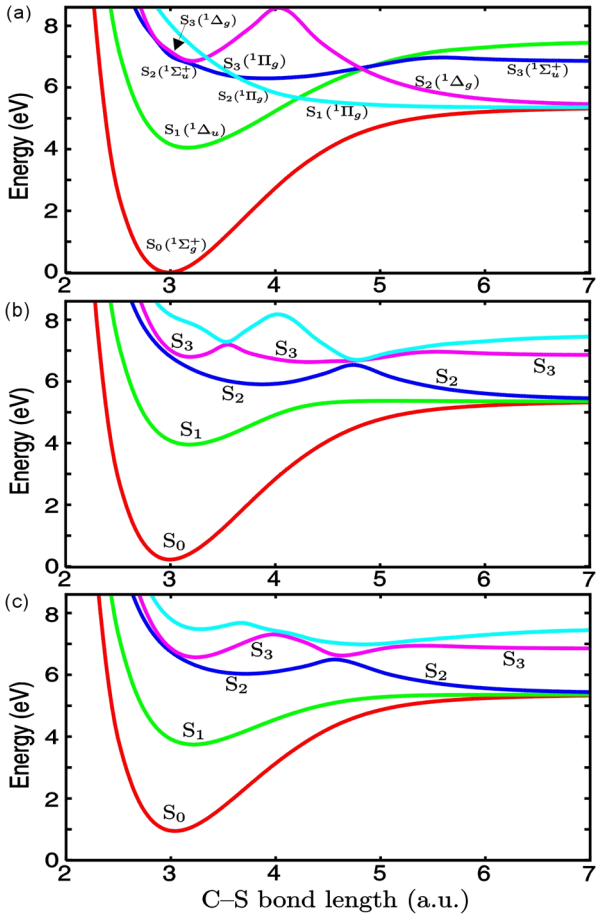

FIG. 1 (color online). Potentials for the lowest few $^1A'$ states of neutral CS_2 along the C–S antisymmetric stretch coordinate for bond angles of (a) 180°, (b) 160°, and (c) 140° with the other C–S bond length fixed at 3.0 a.u. Each color curve represents (a) a diabatic state and (b),(c) an adiabatic state.

dissociation for each cycle. The wave packet begins to transfer from the S_2 adiabatic state to the S_3 adiabatic state at about 35 fs via the conical intersection between the $S_2(^1\Sigma_u^+)$ and $S_3(^1\Pi_g)$ states. More complete details regarding the propagation of these wave packets will be reported in Ref. [31].

To obtain the time-resolved photoelectron spectra, these wave packet densities must be combined with photoionization amplitudes for the underlying electronic states. The initial excited electronic states are represented by the same configuration interaction wave functions employed to construct the potential surfaces shown in Fig. 1. For the final state wave functions (ion plus photoelectron), we assume a frozen-core Hartree-Fock model in which the ion orbitals are taken to be those of the neutral core and the photoelectron orbital is obtained as a solution of a one-electron Schrödinger equation containing the Hartree-Fock potential of the molecular ion. The photoelectron orbital is then expanded in partial-wave form and the partial-wave components are obtained from an iterative solution of the Lippmann-Schwinger equation associated with the one-electron Schrödinger equation. The procedure can provide

converged solutions for the Hartree-Fock photoelectron orbitals and has been successfully used in studies of valence- and K-shell ionization. It has been employed in studies of numerous polyatomic molecules including chloromalonaldehyde [24] and could readily handle molecules with tens of atoms.

We have calculated the time-resolved ion-yield spectra, the time- and energy-resolved photoelectron spectra, and the corresponding molecular-frame angular distributions for ionization of CS_2 by 268 nm photons polarized along the molecular axis (S-S axis). Both the kA' ($^2A''$ ion) and kA'' ($^2A'$ ion) photoelectron continua contribute to these cross sections.

Figure 2(a) shows the measured TRMFPADs with error bars and their best fit (blue) for wave packets prepared on the $C^1\Sigma_u^+$ state of transiently aligned CS_2 with a 201.2 nm pump pulse and ionized by a probe pulse of 268 nm for time delays of 100 and 500 fs [15,21]. The photoelectron energy lies between 0.07 and 0.13 eV. They [15,21] posit that these angular distributions arise from ionization of the π^* orbital in the $C^1\Sigma_u^+$ ($n \rightarrow \pi^*$) state at 100 fs and from a mixture of σ^* and π^* orbitals at 500 fs arising from a nonadiabatic interaction between the $C^1\Sigma_u^+$ state and the $^1\Pi_g$ ($n \rightarrow \sigma^*$) state due to a conical intersection. These distributions are consistent with an atomic picture of ionization of the p component of the π^* orbital into a d ($\ell = 2$) continuum at 100 fs and of ionization of σ^* ($^1\Pi_g$) and π^* ($^1\Sigma_u^+$) orbitals at 500 fs. For comparison, Fig. 2(a) also shows our calculated MFPADs for time delays of 106 and 493 fs convoluted by a Gaussian function with a standard deviation of 15 deg to account for blurring due to the laboratory frame distribution of molecular axes. The calculated and measured spectra are normalized to the same total area. The agreement between these calculated and measured MFPADs at both delay times is encouraging. The calculated angular distributions clearly capture the temporal evolution of the measured spectra, particularly evident in the increase in flux at the poles at $t = 493$ fs and, more subtly, the shifting of the lobes in the MFPAD towards the equator and consequent slight shift in the lobes and broadening at the waist in the alignment distribution averaged result. Differences in the precise form of the calculated and experimental PADs at each time are likely due primarily to experimental artifacts, in particular, spatially inhomogenous background contributions and the instrument response function; further discrepancies may also arise from temporal averaging in the experiment (125 fs pump-probe cross correlation [15]). Although such artifacts will affect the fidelity of the measured PADs and, typically, lead to some loss of angular and temporal structure, they will not affect the gross temporal evolution. Consequently, the experimentally observed temporal trends and their agreement with the calculations are expected to be robust. Finally, we note that further discrepancies may also arise due to the effective temporal characteristics of the pump pulse in the AIMS simulations, since the initial wave packet spread and subsequent evolution are expected to be quite sensitive to this factor.

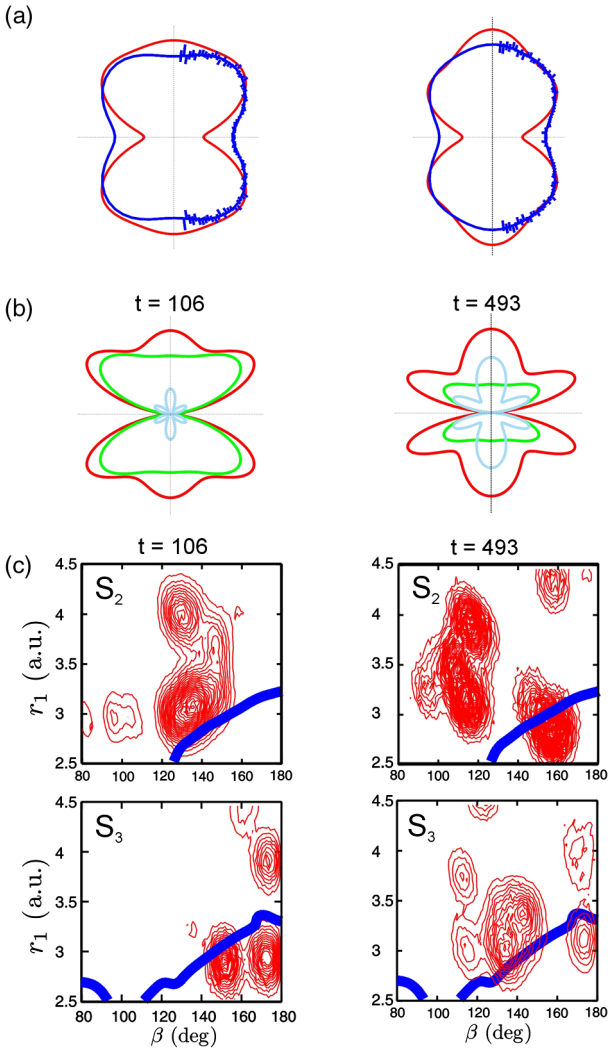

FIG. 2 (color online). (a) Measured MFPADs with error bars (blue bars) and their best fit (blue curves) at time delays of 100 fs (left) and 500 fs (right), and calculated MFPADs convoluted by a Gaussian function with a standard deviation of 15 deg (red) at time delays of 106 fs (left) and 493 fs (right), (b) calculated MFPADs (red) and their contributions from the S_2 state (green) and S_3 state (light blue) at 106 and 493 fs, and (c) the density of the nuclear wave packet on the adiabatic S_2 and S_3 states at 106 and 493 fs. The (blue) banded region in (c) corresponds to the region producing 0.15 eV electrons for r_2 fixed at 3 a.u.

Figure 2(b)shows the calculated total MFPADs (red) and the underlying contributions from ionization of wave packets on the S_2 (green) and S_3 (light blue) surfaces for a delay of 106 and 493 fs and photoelectron energy of 0.15 eV, the strongest peak in the photoelectron spectrum. The contribution to the MFPADs at 106 fs comes mainly from the wave packet on the S_2 state prior to the conical intersection, while the MFPADs at 493 fs arise almost

evenly from wave packets on the S_2 state and from wave packets on the S_3 state that have been transferred nonadiabatically from the S_2 state. A partial wave analysis provides further insight into the response of the MFPADs to the evolving electronic character of the wave packet. The dominant partial waves comprising the calculated MFPADs are found to be consistent with the atomic ionization scheme outlined above. Specifically, the MFPADs arising from the S_2 ($n \rightarrow \pi^*$) state have a dominant d-wave character while those from the S_3 ($n \rightarrow \sigma^*$) state arise from an admixture of p and d waves. These results show clearly how the MFPADs track the nonadiabatic dynamics around a conical intersection in a polyatomic molecule and map the complex evolution of the electronic character of the wave packet.

Examination of the nuclear wave packet in 2(c) provides a complementary description of these observations: at 106 fs, the wave packet is predominantly on the $S_2(^1\Sigma_u^+)$ electronic state, albeit at significantly bent geometries (~140°) displaced from the Franck-Condon region [see Fig. 1(c)], while a small portion of wave packet is nonadiabatically transferred to the $S_3(^1\Pi_g)$ state ionizable around ~150° bent geometries. At 493 fs, the wave packet on the adiabatic S_3 state has accumulated near geometries with a bond angle of ~140° while the wave packet on the S_2 state is near geometries with a bond angle of ~160°, which, as Fig. 1(b) illustrates, corresponds to a region in which the S_2 and S_3 states are close energetically and strongly coupled.

To summarize, these results show that a rigorous description of molecular photoionization, interfaced with wave packet densities obtained from a first-principles multiple spawning simulation, can yield fully *ab initio* determinations of energy-and angle-resolved TRPES spectra that are in impressive agreement with experimentally measured TRMFPADs. The generality of this approach ensures that the technique may be readily employed in the study of diverse molecular systems of photochemical interest.

This work has been supported in part by the National Science Foundation (U.S.) under Grant No. CHE-0956610. These studies also made use of the resources of the Jet Propulsion Laboratory's Supercomputing and Visualization Facility. The authors thank A. Stolow for valuable discussions.

*mckoy@caltech.edu
†Michael.Schuurman@nrc-cnrc.gc.ca

[1] A. Assion, M. Geisler, J. Helbing, V. Seyfried, and T. Baumert, Phys. Rev. A **54**, R4605 (1996).
[2] V. Blanchet, M. Z. Zgierski, T. Seideman, and A. Stolow, Nature (London) **401**, 52 (1999).
[3] J. A. Davies, J. E. LeClaire, R. E. Continetti, and C. C. Hayden, J. Chem. Phys. **111**, 1 (1999).
[4] T. Suzuki, L. Wang, and K. Kohguchi, J. Chem. Phys. **111**, 4859 (1999).
[5] Y. Arasaki, K. Takatsuka, K. Wang, and V. McKoy, J. Chem. Phys. **112**, 8871 (2000).
[6] S. Lochbrunner, T. Schultz, M. Schmitt, J. P. Shaffer, M. Z. Zgierski, and A. Stolow, J. Chem. Phys. **114**, 2519 (2001).
[7] M. S. Schuurman and A. Stolow, in *Conical Intersections: Theory, Computation and Experiment*, edited by W. Domcke, D. Yarkony, and H. Köppel (World Scientific, Singapore, 2011), Chap. 16, pp. 633–667.
[8] R. Schoenlein, L. Peteanu, R. Mathies, and C. Shank, Science **254**, 412 (1991)
[9] L. Hammarstrõm and S. Styring, Phil. Trans. R. Soc. B **363**, 1283 (2008).
[10] R. V. Bensasson, E. J. Land, and T. G. Truscott, *Excited States and Free Radicals in Biology and Medicine* (Oxford University Press, Oxford, England, 1993), Chap. 5.
[11] T. Seideman, J. Chem. Phys. **107**, 7859 (1997).
[12] T. Seideman, Phys. Rev. A **64**, 042504 (2001).
[13] N. Douguet, T. N. Rescigno, and A. E. Orel, Phys. Rev. A **86**, 013425 (2012).
[14] J. G. Underwood and A. Stolow, Adv. Chem. Phys. **139**, 497 (2008).
[15] C. Z. Bisgaard, O. J. Clarkin, G. Wu, A. M. D. Lee, O. Geßner, C. C. Hayden, and A. Stolow, Science **323**, 1464 (2009).
[16] H. R. Hudock, B. J. Levine, A. L. Thompson, H. Satzger, D. Townsend, N. Gador, S. Ullrich, A. Stolow, and T. J. Martínez, J. Phys. Chem. A **111**, 8500 (2007).
[17] C. Ko, A. M. Virshup, and T. J. Martínez, Chem. Phys. Lett. **460**, 272 (2008).
[18] M. Ben-Nun, J. Quenneville, and T. J. Martínez, J. Phys. Chem. A **104**, 5161 (2000).
[19] K. Wang and V. McKoy, Annu. Rev. Phys. Chem. **46**, 275 (1995).
[20] Y. Arasaki, K. Takatsuka, K. Wang, and V. McKoy, J. Chem. Phys. **114**, 7941 (2001).
[21] P. Hockett, C. Z. Bisgaard, O. J. Clarkin, and A. Stolow, Nat. Phys. **7**, 612 (2011).
[22] Y. Arasaki, K. Takatsuka, K. Wang, and V. McKoy, Phys. Rev. Lett. **90**, 248303 (2003).
[23] Y. Arasaki, K. Takatsuka, K. Wang, and V. McKoy, J. Chem. Phys. **119**, 7913 (2003).
[24] M. T. do N. Varella, Y. Arasaki, H. Ushiyama, K. Takatsuka, K. Wang, and V. McKoy, J. Chem. Phys. **126**, 054303 (2007).
[25] Y. Arasaki, K. Takatsuka, K. Wang, and V. McKoy, J. Chem. Phys. **132**, 124307 (2010).
[26] E. J. Heller, J. Chem. Phys. **75**, 2923 (1981).
[27] H. J. Werner, P. J. Knowles, R. Lindh *et al.*, MOLPRO, version 2011.
[28] T. H. Dunning, J. Chem. Phys. **90**, 1007 (1989).
[29] H. Lischka, R. Shepard *et al.*, COLUMBUS, an *ab initio* electronic structure program, release 7.0, 2012.
[30] K. Pierloot, B. Dumez, P.-O. Widmark, and B. O. Roos, Theor. Chim. Acta **90**, 87 (1995).
[31] K. Wang, V. McKoy, M. S. Schuurman, P. Hockett, C. Z. Bisgaard, O. J. Clarkin, and A. Stolow (to be published).